The Journal of Pathology: Clinical Research
J Path: Clin Res April 2014; **1**: 54–65
Published online 17 November 2014 in Wiley Online Library (wileyonlinelibrary.com). DOI: 10.1002/cjp2.5

Original Article

High CerS5 expression levels associate with reduced patient survival and transition from apoptotic to autophagy signalling pathways in colorectal cancer

Seán Fitzgerald,[1,2] Katherine M Sheehan,[3] Virginia Espina,[4] Anthony O'Grady,[3] Robert Cummins,[3] Dermot Kenny,[1,5] Lance Liotta,[4] Richard O'Kennedy,[1,2] Elaine W Kay[3] and Gregor S Kijanka[1]*

[1] *Biomedical Diagnostics Institute, Dublin City University, Dublin, Ireland*
[2] *School of Biotechnology, Dublin City University, Dublin, Ireland*
[3] *Department of Pathology, Royal College of Surgeons in Ireland and Beaumont Hospital, Dublin, Ireland*
[4] *Center for Applied Proteomics and Molecular Medicine, George Mason University, Manassas, VA, USA*
[5] *Molecular and Cellular Therapeutics, The Royal College of Surgeons in Ireland, Dublin, Ireland*

**Correspondence to: Gregor S Kijanka, Biomedical Diagnostics Institute, Dublin City University, Glasnevin, Dublin 9, Ireland.*
e-mail: gregor.kijanka@dcu.ie

Abstract

Ceramide synthase 5 is involved in the *de novo* synthesis of ceramide, a sphingolipid involved in cell death and proliferation. In this study, we investigated the role of ceramide synthase 5 in colorectal cancer by examining ceramide synthase 5 expression, clinico-pathological parameters and association with survival/death signalling pathways in cancer. Immunohistochemical analysis of CerS5 was performed on 102 colorectal cancer samples using tissue microarrays constructed from formalin-fixed and paraffin-embedded tissues. We found strong membranous ceramide synthase 5 staining in 57 of 102 (56%) colorectal cancers. A multivariate Cox regression analysis of ceramide synthase 5 expression adjusted for disease stage, differentiation and lympho-vascular invasion revealed reduced 5-year overall survival ($p = 0.001$) and 5-year recurrence-free survival ($p = 0.002$), with hazard ratios of 4.712 and 4.322, respectively. The effect of ceramide synthase 5 expression on tumourigenic processes was further characterised by reverse phase protein array analysis. Reverse phase protein arrays were generated from laser capture microdissection-enriched carcinoma cells from 19 fresh-frozen colorectal cancer tissues. Measurements of phosphorylation and total levels of signalling proteins involved in apoptosis, autophagy and other cancer-related pathways revealed two distinct signalling networks; weak membranous ceramide synthase 5 intensity was associated with a proteomic network dominated by signalling proteins linked to apoptosis, whereas strong ceramide synthase 5 intensity was associated with a proteomic sub-network mostly composed of proteins linked to autophagy. In conclusion, high ceramide synthase 5 expression was found in colorectal cancer tissue and was associated with poorer patient outcomes. Our findings suggest that this may be mediated by a transition from apoptotic to autophagy signalling pathways in ceramide synthase 5 High expressing tumours, thus implicating ceramide synthase 5 in the progression of colorectal cancer.

Keywords: ceramide synthase 5; colorectal cancer; prognosis; apoptosis; autophagy; reverse phase protein arrays; laser capture microdissection

Received 20 June 2014; accepted 28 August 2014
Conflict of interest: The authors have declared no conflicts of interest.

Introduction

Ceramide synthases 1-6 (CerS1-6) are a family of enzymes involved in *de novo* synthesis of ceramides from sphingoid bases and acyl-CoA substrates and in the endoplasmic reticulum of mammalian cells [1]. Each enzyme is unique that it generates bioactive ceramides of specific fatty acid chain lengths. These ceramides are implicated in apoptosis, cell proliferation and autophagy [2]; however, the exact mechanism by which individual ceramides contribute to these processes remains largely unknown. Although ceramides are generally assumed to be pro-apoptotic [3,4], recent findings suggest that elevated levels of

ceramides increase tumour growth in severe combined immune-deficient (SCID) mice, while silencing of the CerS6 gene leads to apoptosis in cancer cell lines [5,6]. The implication that ceramides can cause both tumour-promoting or tumour-suppressing effects in different cell types may reflect the cell of origin, ceramide chain lengths and the tissue expression levels of specific CerS enzymes, thus playing a key role in the regulation of tumourigenesis.

In the current study, we specifically investigated the role of CerS5 in colorectal cancer (CRC) based on our previous work, whereby, CerS5 was found to be unregulated on a gene level in CRC patients [7]. CerS5 is expressed ubiquitously in mammalian tissue in an organ specific distribution pattern [8,9]; however, its expression in cancer tissue is less well characterised. Recent studies have shown that reduced gene expression levels of CerS2, CerS4 and CerS6 are associated with tumour grade, lymph node status and cell proliferation in breast cancer [10–12]; while in head and neck tumours, CerS1 has been shown to negatively regulate tumour growth [13]. While most of these studies were based on gene expression analysis and silencing studies of specific CerS enzymes, we aimed to monitor the protein expression levels of CerS5 in human CRC tissue and correlate these with clinico-pathological data.

Materials and methods

Patient characteristics, tissue specimens and study design

The study was approved by the Ethics (Medical) Research Committee at Beaumont Hospital, Dublin, Ireland, and informed consent was obtained from all patients. Patients undergoing colonoscopy were screened prospectively, with exclusion of patients with history of cancer, inflammatory bowel disease and colorectal cancer patients undergoing neoadjuvant therapy. A total of 121 cases with a diagnosis of colorectal cancer (CRC) met the inclusion criteria and were included in the study. The median age of the patients at the time of first diagnosis was 69.5 (range 34–88 years). The cohort included 72 male and 49 female patients. In total, 83 patients had colonic carcinoma, while 38 had rectal carcinomas. Patients were subdivided into two cohorts; 102 patients with colorectal cancer diagnosed between 2001 and 2007 with a minimum 5-year follow-up were included to the immunohistochemistry arm of the study (IHC cohort) which aimed at examining CerS5 expression in archived formalin-fixed and paraffin-embedded (FFPE) tissue. Statistical power of the IHC cohort was calculated retrospectively with a power value of 1-beta = 0.99. In order to characterise the signalling protein networks associated with CerS5, we performed reverse phase protein array (RPPA) analysis in fresh-frozen tissue from additional 19 patients with colorectal cancer (RPPA cohort). Statistical power of the RPPA cohort was calculated retrospectively with a power value of 1-beta = 0.83. Patients in the RPPA cohort were diagnosed with colorectal cancer between 2012 and 2013 and met the same inclusion criteria as those of the IHC cohort. Clinical and pathological parameters of all patients are presented in Table 1.

Local resection and a standard fixation protocol were carried out in all cases and the specimens were selected to represent all colorectal cancer stages and histological types. A pathologist identified and collected an area of invasive carcinoma from the tumour mass and an adjacent area of uninvolved colonic/rectal mucosa for formalin fixation and paraffin embedding. Each block was sectioned and stained with haematoxylin and eosin and graded by a consultant pathologist (EWK) to confirm pathological stage and grade of the tumours. Relevant tumour areas were marked for tissue microarray construction. All fresh tissue samples for RPPA analysis were processed uniformly and rapidly to ensure preservation of molecular endpoints and snap-frozen in liquid nitrogen. The time from removal of a colectomy specimen to snap-freezing of samples was <20 min. Fresh-frozen tissue samples were stored at -80°C.

Tissue microarrays and immunohistochemistry

The tissue microarray (TMA) construction was performed as previously described [14,15], using the Beecher Instruments Tissue Microarrayer (Beecher Instruments, Silver Spring, MD, USA). Cores of 1.0 mm diameter were collected in quadruplicate for each case. A total of 100 out of 102 cases of the IHC cohort were incorporated into the TMAs and two further cases were investigated as whole tumour sections for additional staining homogeneity assessment. All 19 cases of the RPPA cohort were also investigated for CerS5 expression using IHC in FFPE whole tissue sections. Finally, a TMA with 24 normal mucosa cases from surgical margins and further cohort of ten normal whole sections from surgical margins were used to assess the CerS5 staining in normal tissue.

Sections of 4 μm thickness were cut from all TMA blocks and the whole section blocks for immunohistochemistry. Sections were immunostained with an

Table 1. Clinico-pathological details of patient cohorts

Factor	IHC cohort		RPPA cohort	
	Number of patients	%	Number of patients	%
	102	100	19	100
Gender				
Female	39	38.2	10	52.6
Male	63	61.8	9	47.4
Age (years)				
Median	70	–	67	–
Range	34–87	–	47–88	–
<65	40	39.2	8	42.1
≥65	62	60.8	11	57.9
Tumour site				
Colon	68	66.7	15	78.9
Rectum	34	33.3	4	21.1
Tumour stage*				
T1	8	7.8	0	0
T2	16	15.7	0	0
T3	63	61.8	13	68.4
T4	13	12.7	6	31.6
Not Stated†	2	2	–	–
Node stage*				
N0	60	58.8	11	57.9
N1	22	21.6	2	10.5
N2	18	17.6	6	31.6
Not Stated†	2	2	–	–
Metastasis stage*				
M0	91	89.2	17	89.5
M1	11	10.8	2	10.5
Lymphovascular invasion				
Yes	25	25	7	36.8
No	77	75	12	63.2
Differentiation				
Well	2	2	0	0
Moderately	88	86.3	17	89.5
Poorly	12	11.7	2	10.5
Follow-up (months)				
Median	59	–	N/A‡	–
Range	1–122	–	N/A‡	–

T, tumour; N, node; M, metastasis.
*TNM were staged according to the 5th edition of the AJCC Cancer Staging Manual.
†These patients presented with terminal metastatic disease and only had biopsies taken; thus, their T and N stages could not be accurately determined.
‡Follow-up information was not available for these patients as they were diagnosed with CRC in 2012/2013.

anti-CerS5 human polyclonal antibody (pAb) (LS-B3152, LifeSpan Biosciences, Inc. Seattle, WA, USA) on an automated platform (Bond system – Leica Microsystems, Bannockburn, IL, USA). Briefly, cut sections were subjected to on-board dewaxing and the following conditions were applied: CerS5 antigen retrieval in tri-sodium citrate buffer (Bond Epitope Retrieval 1 solution) for 20 min and 1:300 antibody dilution. Detection of the antibody–antigen complex was achieved using a polymer-based kit (Bond Refine) with 3,3'-diaminobenzidine (DAB) as the chromogen. All sections were counterstained with haematoxylin. Negative controls were included for all sections by omitting the primary antibody and positive control tissue included tonsil and colonic adenocarcinoma. Whole-cell lysates were prepared from human colon cancer cell line SW620 and standard western blot analysis was conducted as a positive control for the CerS5 (LS-B3152) antibody (supplementary material Figure S2.

Immunohistochemical evaluation was performed independently by two reviewers blinded to the clinico-pathological details and clinical outcomes of the cohort. An intensity score was assigned to each core within the TMA and a representative score was assigned to each whole section based on the intensity of the staining in the majority of the positive cells. The degree of membranous CerS5 staining was evaluated and the intensity (negative = 0; weak = 1+; moderate = 2+; strong = 3+) was recorded. Intensities 0 & 1+ were defined as IHC CerS5 Low and 2+ and 3+ were defined as IHC CerS5 High as previously shown [16,17]. The homogeneity of the staining between TMA cores and inter-observer variability was assessed as previously shown [18]. In cases where there were discrepancies between the scorers, a consensus was reached after a joint review using a multi-headed microscope.

Laser capture microdissection and reverse phase protein arrays

Laser capture microdissection (LCM) was performed to enrich epithelium and remove stroma for cell signalling analysis as described previously [19,20]. Briefly, 8 μm frozen tissue sections were obtained for each sample from consecutive cryostat sections and approximately 20,000 epithelial cells (approximately 15 000–20 000 laser shots) were removed for each frozen tissue sample, using an infrared-based laser capture system (Arcturus *XT*, Life Technologies, San Francisco, CA, USA). No attempt was made to target specific regions of carcinoma cells within the tumour and multiple separate areas of tissue were dissected so that signalling analysis could be performed on a cell population-wide scale within each patient sample. Micro-dissected cells were lysed in 30 μl of lysis buffer containing a 1:1 mixture of Tris–Glycine SDS sample buffer (Invitrogen, Life Technologies, Carlsbad, CA, USA) and Tissue Protein Extraction Reagent (T-PER), (Pierce, Rockford, IL, USA) solution supplemented with 100 μl of Bond Breaker TCEP (Tris(2-carboxyethyl)phosphine) solution, (ThermoFisher Scientific, Rockford, IL, USA). Tissue processing and preparation of tissue lysates have been described previously [21,22].

RPPA were generated as described previously [23–26]. LCM-enriched epithelium lysates were printed in triplicate on ONCYTE Avid nitrocellulose film-slides (GRACE Bio-Labs, Bend, OR, USA) using an Aushon 2470 arrayer equipped with 350 μm pins (Aushon Biosystems, Billerica, MA, USA). Each array contained epithelium lysates for all 19 cases and each lysate was printed in a two-fold dilution curve representing undiluted lysate, 1:2, 1:4 and 1:8 dilutions. Control lysates were printed in a two-fold dilution curve. All RPPAs were baked for 2 h at 80°C to allow fixation and then stored with desiccant at −20°C. Quality control samples, including A431 cell lines (±EGF stimulation; BD Pharmingen, San Diego, CA, USA) and a pooled sample from CRC cases included in this study, were printed on the RPPA to ensure protein deposition and immunostaining reactivity [27].

RPPA immunostaining, image acquisition and data analysis

RPPA slides were blocked (I-Block, Applied Biosystems, Carlsbad, CA, USA) for 2 h before immunostaining. Immunostaining was conducted on a Dako Autostainer (Catalyzed Signal Amplification kit, Dako, Carpinteria, CA, USA). Each slide was incubated with a single primary antibody at room temperature for 30 minutes. The negative control slide was incubated with antibody diluent (Dako). For each immunostaining run, 1 slide was incubated with anti ssDNA antibody (1:15 000; IBL International GmbH). Secondary antibody was goat anti-rabbit (1:10 000; Vector Laboratories), or rabbit anti-mouse IgG (1:10; Dako), which were amplified via horseradish peroxidase-mediated biotinyl tyramide with chromogenic detection (diaminobenzidine; Dako). In total, 30 primary antibodies specific to known signalling endpoints were used to measure phosphorylation and protein levels using RPPAs (supplementary material Table S1). Two additional slides were stained with Sypro Ruby Protein Blot Stain (Molecular Probes, Eugene, OR, USA) and visualized with NovaRay Image Acquisition Software (Alpha Innotech, San Leandro, CA, USA) to determine the total protein concentrations.

RPPA slides were scanned on a UMAX 2100XL flatbed scanner (white balance 255, black 0, middle tone 1.37, 600 dpi, 14 bit). Spot intensity was analysed by Image Quant v5.2 software (Molecular Dynamics, Sunnyvale, CA, USA). Data reduction was carried out with a VBA Excel macro, RPPA Analysis Suite [28]. To normalize data, the relative intensity for each protein spot was divided by the ssDNA relative intensity for the corresponding spot [29].

Proteomic network analysis

Proteomic network analysis was performed as previously shown [30]. Briefly, Spearman ρ correlation analysis with $\rho \geq 0.75$ and $p \leq 0.01$ was used to build proteomic network graphs (Gephi 0.8.2 beta, The Gephi Consortium, Paris, France, www.gephi.org). Proteomic networks were drafted based on two CRC patient groups classified by their clinical outcomes derived from the IHC cohort; IHC CerS5 Low group representing good prognosis and IHC CerS5 High group representing poor prognosis. Nodes in the networks represent RPPA endpoint molecules; the bigger the node, the more the significant correlations relative to the molecule. Each line connecting two nodes represents a significant correlation between the nodes; the thicker the line, the higher the Spearman ρ correlation. Proteins are grouped on the basis of Spearman ρ values and the number of connections among a group of nodes; strongly correlated nodes are represented close to each other and with the same colour.

Statistical analysis

Sample size power analysis was performed retrospectively using GPower 3.1 software for a two-tailed t-test (point biserial model). Effect size (0.0549), sample size (102) and alpha (0.05) were given for the IHC cohort and (0.0579), (19) and (0.05), respectively, for the RPPA cohort. Power value of 1-beta > 0.8 was considered statistically adequate. Association between discrete variables was assessed using the χ^2 test. Five-year survival and 5-year recurrence-free survival were analysed and survival curves were plotted according to the Kaplan-Meier method using the generalized log-rank test to compare survival curves. Prognostic factors for 5-year survival and 5-year recurrence-free survival were evaluated by univariate and multivariate analyses for tumour, node, metastasis (TNM) stages, gender, differentiation and lymphovascular invasion (Cox proportional hazard regression model). For both Kaplan-Meier and Cox regression analyses, patients who had follow-up information for more than 5 years were censored at 5 years post-diagnosis. All tests were analysed using SPSS 19.0 software (SPSS, Chicago, IL, USA) and the findings were considered statistically significant at $p < 0.05$. Unsupervised hierarchical clustering of the RPPA dataset was conducted using JMP 5.1.2 (SAS Institute Inc., Cary, NC, USA). The Spearman rank correlation coefficient, ρ, was calculated for each protein pair in the RPPA cohort; $\rho \geq 0.75$ with $p \leq 0.01$ was considered significant.

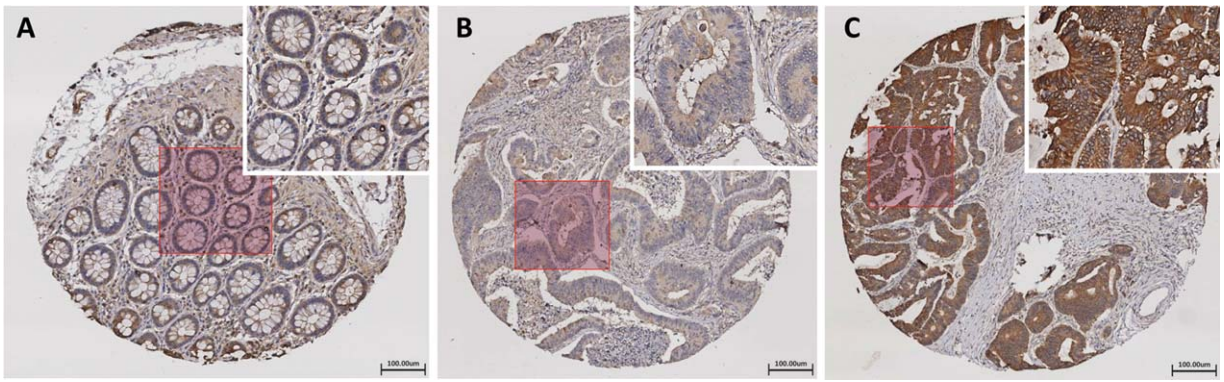

Figure 1. IHC staining for CerS5 in colorectal adenocarcinoma and normal colorectal mucosa. (A) Normal colorectal mucosa from tumour-free adjacent surgical margins with negative membranous CerS5 staining. (B) Colorectal cancer tissue with weak membranous CerS5 staining. (C) Colorectal cancer tissue with strong membranous CerS5 staining.

Results

CerS5 is expressed in both normal and cancerous colorectal tissue

In previous studies, we showed that CerS5 is upregulated on a gene level in colorectal cancer [7]. Although CerS5 has been shown to be expressed at low basal levels in most non-cancerous tissues, studies have yet to show protein expression of CerS5 in colorectal cancer. Our results show distinct membranous CerS5 staining in both the normal mucosa and cancerous tissue (Figure 1). High membranous CerS5 staining intensity (2+ and 3+) was found in 55.9% (19/34) of cancerous tissue samples when compared with patient-matched adjacent normal mucosa. Low CerS5 staining (0 and 1+) was observed in 45.1% (46/102) and high CerS5 staining (2+ and 3+) was observed in 54.9% (56/102) of CRC patient tissue in the IHC cohort. No correlation was found between CerS5 staining intensity and standard prognostic variables in the IHC cohort (see supplementary material Table S2). The RPPA cohort was also evaluated by immunohistochemistry in FFPE tissue with 42.1% (8/19) CRC tumours demonstrating low staining intensity (0 and 1+) and 57.9% (11/19) showing high (2+ and 3+) staining intensity of CerS5.

High CerS5 expression in colorectal cancer tissue correlates with poor patient survival

To assess if CerS5 staining intensity correlated with patient survival, we analysed the 5-year follow-up data of the 102 cases in our IHC cohort. Kaplan-Meier analysis showed that high CerS5 staining in colorectal cancer was found to have a significant negative prognostic value (Figure 2). Overall 5-year survival rates for patients with high CerS5 membranous intensity were significantly lower than those with low CerS5 membranous intensity ($p = 0.001$; Figure 2A). Five-year recurrence-free survival was also significantly lower for patients with high CerS5 membranous intensity, when compared with those showing low CerS5 membranous intensity ($p = 0.002$; Figure 2B).

CerS5 expression is an independent predictor of survival and disease recurrence

Multivariate analysis showed that the intensity of membranous CerS5 expression was an independent predictor of 5-year overall survival and 5-year recurrence-free survival ($p = 0.019$ and $p = 0.011$, respectively) in CRC patients (Table 2). Membranous CerS5 expression was independent of TNM stage, gender, differentiation and lymphovascular invasion in its ability to predict prognosis. The hazard ratio for 5-year overall survival in patients with high CerS5 expression was 4.7 times higher than in CerS5 low patients and for 5-year recurrence-free survival the hazard ratio in CerS5 high patients was 4.3 times higher than in CerS5 low patients.

Unsupervised hierarchical clustering analysis identifies two distinct groups of patients

On the basis of the results thus far, we sought to understand the underlying molecular interplay associated with the significant effects of CerS5 expression levels on patient outcomes. We therefore applied our RPPA cohort to investigate protein networks associated with sphingolipid metabolism, apoptosis, autophagy and other cancer related pathways in CerS5 high and low tumours. Thirty antibody substrates (see

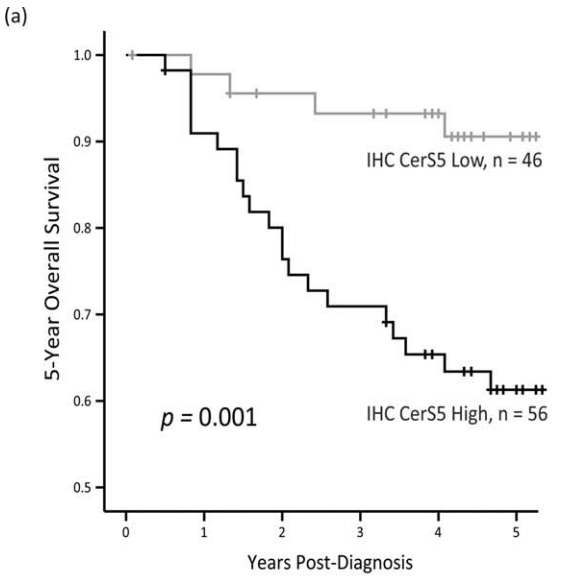

No. at risk	0	1	2	3	4	5
CerS5 Low	46	44	41	40	35	25
CerS5 High	56	50	42	39	33	25

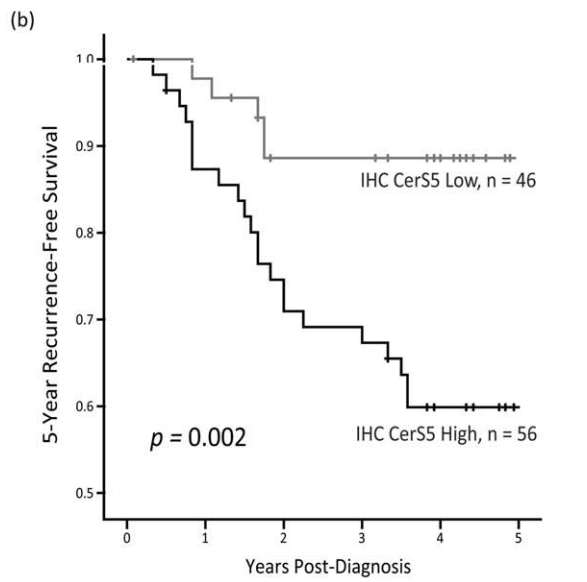

No. at risk	0	1	2	3	4	5
CerS5 Low	46	44	37	37	32	23
CerS5 High	56	48	39	37	30	25

Figure 2. High CerS5 expression is associated with poor prognosis in CRC. (A) Kaplan–Meier analysis revealed that high CerS5 expression correlates significantly with lower 5-year overall survival (log-rank test, $p = 0.001$) and (B) lower 5-year recurrence-free survival (log-rank test, $p = 0.002$).

supplementary material Tables S1 and S3) were quantified in the RPPA patient cohort for proteomic analysis. Unsupervised hierarchical clustering analysis of RPPA signalling endpoint measurements identified two distinct clusters as represented by a heat map in Figure 3. These two clusters support the results seen by immunohistochemical analyses; the first cluster (red) on the dendrogram is composed mainly of IHC CerS5 High patients (nine cases) and with three IHC CerS5 Low patients. The second cluster on the dendrogram (green) contains mainly IHC CerS5 Low patients (five cases) with two IHC CerS5 High cases. Whereas the green cluster is largely uniform, with low to intermediate relative signal intensities of the investigated signalling endpoints, the red cluster is more heterogeneous, further subdividing into a low to intermediate intensities sub-cluster of seven patients (five IHC CerS5 High and two IHC CerS5 Low) and an intermediate to high intensities sub-cluster of five patients (four IHC CerS5 High and one IHC CerS5 Low).

IHC CerS5 High and Low proteomic networks differ in colorectal cancer

We next used Spearman ρ rank correlation analyses to determine significant protein interactions identified by RPPA measurements. The analysis of 30 signalling endpoints revealed that 49 of 435 protein pairs were positively and significantly correlated ($\rho > 0.75$, $p \leq 0.01$) in both IHC CerS5 High and Low patients (see supplementary material Tables S4 and S5). Sixty-three positive significant correlations were found exclusively in the IHC CerS5 Low group (Figure 4A; supplementary material Table S4), whereas 54 protein pairs showed a significant Spearman ρ value exclusively in the IHC CerS5 High group (Figure 4B; supplementary material Table S5). We did not observe any significant RPPA protein interactions that correlated negatively. The protein interaction network of colorectal cancer specimens associated with a IHC CerS5 High staining intensity was distinctly different from the IHC CerS5 Low network (Figure 4).

IHC CerS5 Low proteomic network is associated with apoptosis

The IHC CerS5 Low proteomic network constructed from the Spearman ρ rank correlation analyses revealed four main sub-networks (Figure 4A). The sub-networks were defined by proteins strongly correlated and in close proximity to each other and these were represented by the same colour in the network. The four main CerS5 low sub-networks were dominated by proteins linked to apoptosis, including PP2A, survivin and the cleaved caspases 3

Table 2. Cox univariate and multivariate regression analyses of overall and recurrence-free survival

	Univariate				Multivariate			
			95% CI for HR				95% CI for HR	
Variable	*p* Value	HR	Lower	Upper	*p* Value	HR	Lower	Upper
5-Year overall survival								
CerS5 High/Low	0.004	4.855	1.666	14.152	0.019	4.712	1.287	17.250
Gender	0.460	1.373	0.592	3.183	0.939	1.040	0.382	2.829
T-stage	0.000	4.062	1.984	8.317	0.053	2.226	0.989	5.007
N-stage	0.002	2.017	1.284	3.170	0.530	1.259	0.613	2.587
M-stage	0.000	8.140	3.515	18.851	0.464	1.600	0.455	5.620
Differentiation	0.000	4.903	2.037	11.801	0.041	3.165	1.049	9.547
Lymphovascular invasion	0.001	3.612	1.642	7.946	0.381	1.715	0.514	5.721
5-Year recurrence-free survival								
CerS5 High/Low	0.005	4.047	1.532	10.690	0.011	4.322	1.407	13.280
Gender	0.551	1.275	0.573	2.840	0.870	1.079	0.434	2.681
T-stage	0.002	2.809	1.455	5.424	0.131	1.721	0.851	3.479
N-stage	0.004	2.883	1.221	2.903	0.677	1.152	0.591	2.246
M-stage	–	N/A*	–	–	–	N/A*	–	–
Differentiation	0.002	3.920	1.667	9.224	0.046	2.667	1.018	6.987
Lymphovascular invasion	0.001	3.455	1.621	7.362	0.132	2.359	0.773	7.194

HR, Hazard Ratio; CI, confidence interval; T, tumour; N, node; M, metastasis.
*Five-year recurrence-free survival analysis not applicable for patients with metastatic disease.

and 7. These dominant nodes radiated outward to interconnect with other cancer associated molecules within their respective sub-networks. These results provide evidence for the activation of the ceramide driven apoptotic pathways in CerS5 low tumours, potentially resulting in better outcomes seen in colorectal cancer patient with weak membranous CerS5 staining.

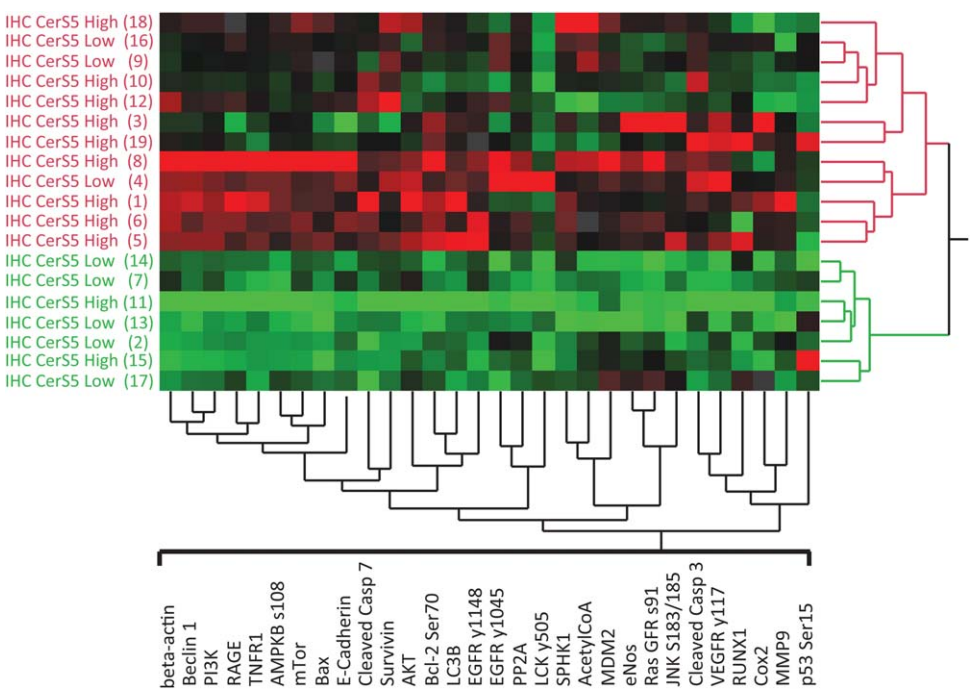

Figure 3. Unsupervised hierarchical cluster analysis in 19 CRC patients based on RPPA measurements of 30 endpoints. Patients (IHC CerS5 High and Low) are shown on the vertical axis, 30 endpoints are outlined on the horizontal axis. Higher relative levels of signal are represented in red; intermediate in black and lower levels are in green. The analysis identifies two groups of patients; the first cluster (red) is mainly composed of IHC CerS5 High patients, whereas the second cluster contains mainly IHC CerS5 Low patients.

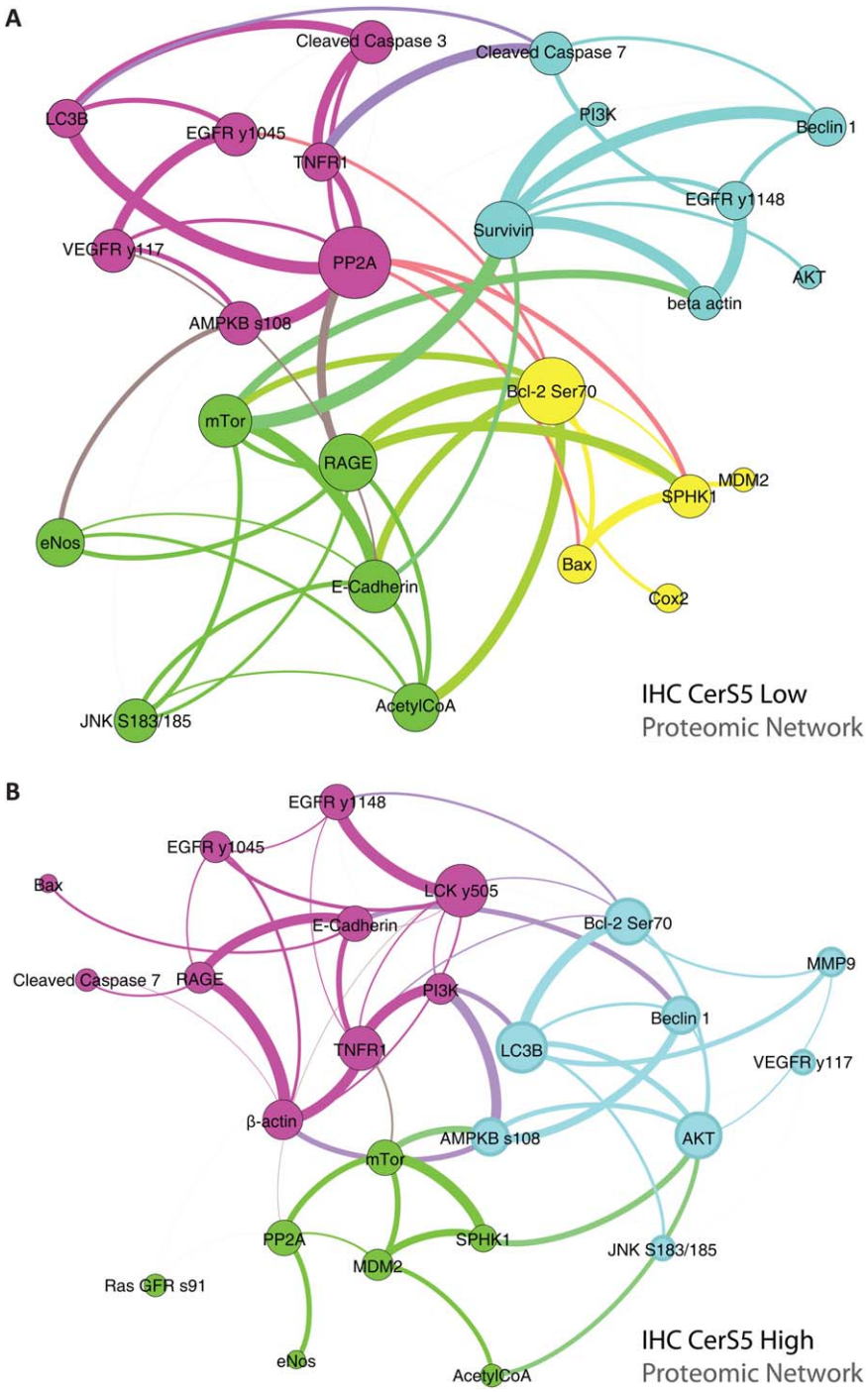

Figure 4. RPPA analysis identifies distinct proteomic networks in IHC CerS5 High and Low CRC patients. (A) IHC CerS5 Low proteomic network consists of four main sub-networks dominated by proteins linked to apoptosis; including PP2A, survivin and the cleaved caspases 3 and 7. (B) IHC CerS5 High proteomic network consists of three sub-networks with one sub-network mainly composed of proteins linked to the autophagy (blue); including the initiators of autophagy beclin 1 and JNK and the autophagy regulators Akt, AMPK and LC3B.

IHC CerS5 High proteomic network is associated with autophagy

The IHC CerS5 High proteomic network was composed of three main sub-networks as shown in Figure 4B. When we compared the IHC CerS5 IHC CerS5 High and Low proteomic networks, we found that the IHC CerS5 High network is not dominated by proteins associated with apoptosis, as seen in the

IHC CerS5 Low network. However, in CerS5 high patients, we identified one sub-network mostly composed of proteins linked to the autophagy (Figure 4B, light blue). The autophagy sub-network is composed of the initiators of autophagy beclin 1 and JNK and the autophagy regulators Akt, AMPK and LC3B. Interestingly, the autophagy sub-network is linked through mTOR, to the sphingolipid metabolism proteins PP2A and SPHK1, both associated with autophagy through mTOR pathway activation [31]. Taken together, these results suggest a dysregulation of the ceramide-driven apoptotic pathways and activation of autophagy in CerS5 high patients, which may account for the correlation of strong CerS5 expression and poor survival.

Discussion

Our results indicate that strong CerS5 staining correlates with poor prognosis in patients with CRC. A favourable prognosis was observed in CRC patients with weak CerS5 staining, which was also found in the majority of normal colorectal mucosae. This data suggests that elevated CerS5 expression is associated with increased tumour aggressiveness, which may be regulated by altered levels of bioactive ceramides, through mechanisms that have yet to be elucidated. Interestingly, altered expression levels of CerS in colon cancer may distort the balance of ceramides, thereby contributing to tumour progression [12]. Proteomic network analysis in this study demonstrates a shift from apoptosis-related pathways in CerS5 low cases to autophagy in CerS5 high cases, suggesting a causative link between poor survival in CerS high cases and a dysregulation of programmed cell-death pathways.

Our previous work identified CerS5 as a marker in CRC and showed that it is upregulated on a gene level [7]. In the current study, we confirmed elevated CerS5 on a protein level in CRC tissue using immunohistochemistry. Other studies have shown CerS5 expression at low basal levels in non-cancerous tissues [8,9]; however, there is a paucity of literature on protein expression of CerS5 in cancer tissue. It has been shown that downregulation of the CerS2 gene in breast cancer is associated with poor patient outcomes [32]. In addition, the overexpression of specific enzymes of sphingolipid metabolism has been shown to have both a negative prognostic value (ceramide kinase) and a positive prognostic value (galactosyl ceramide synthase, ganglioside GD3 synthase) in breast cancer [33].

Ceramides are generally assumed to be pro-apoptotic [3,4]; and as such, one would expect that increased CerS levels would lead to increased ceramides in tumour tissue with resultant cell death. However, the data presented in our study suggests that strong staining of CerS5 in CRC tissue is tumour progressive. Recent studies support our findings demonstrating that elevated levels of ceramides increase tumour growth in SCID mice, and that silencing rather than overexpression of the CerS6 gene can lead to apoptosis in cancer cell lines [5,6]. Furthermore, Hartmann *et al*, demonstrated that overexpression of CerS2, despite having no direct impact on ceramide levels, leads to increased cell proliferation in breast and colon cancer cell lines [12]. These studies in conjunction with our findings suggest that although apoptosis is a recognised feature of ceramides, specific CerS expression levels and ceramide fatty acid chain lengths in different tissues may provide alternative survival modes in cancer.

The proteomic data presented in our study may offer some insights into the tumour suppressive and tumour promoting effects of CerS5 in CRC. Analysis of the RPPA data revealed two distinct signalling networks for CerS5; an IHC CerS5 Low proteomic network associated with apoptosis and an IHC CerS5 High proteomic network associated with autophagy. The apoptotic pathway, which emerged from our IHC CerS5 Low network, included apoptosis-related proteins such as PP2A, survivin and caspases 3 and 7. Veret *et al*, recently showed that overexpression of CerS4 in pancreatic β-cells induced apoptosis and was associated with increased caspase 3 and 7 activities through *de novo* synthesis of C18 ceramide species [4]. By contrast, another study showed that down-regulation of CerS6 in SCID mice was linked to caspase 3 activation and subsequent apoptosis [6]. In our IHC CerS5 High proteomic network, LC3B, beclin 1 and JNK were identified as key signalling molecules for autophagy, a phagolysosome process whereby damaged proteins and organelles are removed to prevent cell damage and intracellular molecules are sequestered for cell survival [34]. Espina *et al* have recently shown that autophagy is required to promote abnormal breast cancer progenitor cells into invasive breast cancer by providing necessary survival mechanisms under stress [35]. Another study in pancreatic cancer showed that autophagy was required for tumour growth [36]. LC3B dominates a central node in the IHC CerS5 High network and has been previously been shown to induce mitochondrial autophagy in human cancer cells by directly binding to ceramides [37]. Although CerS5 has not been linked to autophagy in cancer, a

model of diabetic cardiomyopathy showed that CerS5 promoted cardiac autophagy through de novo synthesis of C14-ceramide [38]. Furthermore, cardiac autophagy required CerS5 for sphingolipid-mediated induction of beclin 1 protein and overexpression of LC3B, both of which dominate central nodes in our CerS5 high proteomic network.

Although we have outlined two distinct signalling networks associated with apoptosis and autophagy, there are, however, dominant nodes common to both networks such as Bcl-2 and SPHK1. This may be explained by the fact that apoptosis and autophagy are intimately linked through common signalling pathways. Binding of Bcl-2 to phosphorylated beclin 1 induces autophagy while cleavage of beclin 1 by effector caspases is pro-apoptotic [39]. Sphingosine kinase 1 (SPHK1), a central enzyme in sphingolipid metabolism, activates anti-apoptotic signal transduction in a model of Kaposi's sarcoma in SCID mice [40]; while other studies have shown that overexpression of SPHK1 stimulates autophagy in breast cancer cells by increasing the formation of LC3B-positive autophagosomes [41].

In conclusion, we show for the first time that CerS5 is overexpressed in CRC tissue on protein level and that CerS5 high expression is associated with poor patient survival. We delineated two distinct CerS5 signalling networks, which may influence the fate of the cancer cell by switching between apoptosis and autophagy. This study highlights the importance of ceramide synthases in the tumourigenic process and that selective targeting of products of sphingolipid metabolism may prove beneficial in the therapeutic treatment of colorectal cancer.

Acknowledgements

We gratefully acknowledge the help of Dr. Joanna Fay, Deirdre Hyland and our surgical colleagues in Beaumont Hospital and Martin Somers from the Biomedical Diagnostics Institute for his help in editing of illustrations. This work was supported by grants from the Irish Cancer Society CRF10KIJ, the Science Foundation Ireland 10/CE/B1821 and Pathological Society Visiting Fellowship VF 2013/04/01.

Author contributions

Study conception and design: EWK, GSK; acquisition of data: SF, KMS, VE, AO'G, RC, GSK; analysis and interpretation of data: SF, KMS, VE, AO'G, DK, LL, RO'K, EWK, GSK; drafting of the manuscript: SF, GSK; revision of the manuscript: KMS, VE, AO'G, RC, DK, LL, RO'K, EWK, GSK. The final version of the manuscript has been reviewed and approved by all authors.

References

1. Mullen TD, Jenkins RW, Clarke CJ, *et al*. Ceramide synthase-dependent ceramide generation and programmed cell death: involvement of salvage pathway in regulating postmitochondrial events. *J Biol Chem* 2011; **286**: 15929–15942.
2. Morad SAF, Cabot MC. Ceramide-orchestrated signalling in cancer cells. *Nat Rev Cancer* 2013; **13**: 51–65.
3. Bose R, Verheij M, Haimovitz-Friedman A, *et al*. Ceramide synthase mediates daunorubicin-induced apoptosis: an alternative mechanism for generating death signals. *Cell* 1995; **82**: 405–414.
4. Veret J, Coant N, Berdyshev EV, *et al*. Ceramide synthase 4 and de novo production of ceramides with specific N-acyl chain lengths are involved in glucolipotoxicity-induced apoptosis of INS-1 beta-cells. *Biochem J* 2011; **438**: 177–189.
5. Senkal CE, Ponnusamy S, Bielawski J, *et al*. Antiapoptotic roles of ceramide-synthase-6-generated C16-ceramide via selective regulation of the ATF6/CHOP arm of ER-stress-response pathways. *FASEB J* 2010; **24**: 296–308.
6. Senkal CE, Ponnusamy S, Manevich Y, *et al*. Alteration of ceramide synthase 6/C16-ceramide induces activating transcription factor 6-mediated endoplasmic reticulum (ER) stress and apoptosis via perturbation of cellular Ca2+ and ER/Golgi membrane network. *J Biol Chem* 2011; **286**: 42446–42458.
7. Kijanka G, Hector S, Kay EW, *et al*. Human IgG antibody profiles differentiate between symptomatic patients with and without colorectal cancer. *Gut* 2010; **59**: 69–78.
8. Levy M, Futerman AH. Mammalian ceramide synthases. *IUBMB Life* 2010; **62**: 347–356.
9. Mullen TD, Hannun YA, Obeid LM. Ceramide synthases at the centre of sphingolipid metabolism and biology. *Biochem J* 2012; **441**: 789–802.
10. Ruckhaberle E, Holtrich U, Engels K, *et al*. Acid ceramidase 1 expression correlates with a better prognosis in ER-positive breast cancer. *Climacteric* 2009; **12**: 502–513.
11. Schiffmann S, Sandner J, Birod K, *et al*. Ceramide synthases and ceramide levels are increased in breast cancer tissue. *Carcinogenesis* 2009; **30**: 745–752.
12. Hartmann D, Lucks J, Fuchs S, *et al*. Long chain ceramides and very long chain ceramides have opposite effects on human breast and colon cancer cell growth. *Int J Biochem Cell Biol* 2012; **44**: 620–628.
13. Koybasi S, Senkal CE, Sundararaj K, *et al*. Defects in cell growth regulation by C18:0-ceramide and longevity assurance gene 1 in human head and neck squamous cell carcinomas. *J Biol Chem* 2004; **279**: 44311–44319.
14. Kay E, O'Grady A, Morgan JM, *et al*. Use of tissue microarray for interlaboratory validation of HER2 immunocytochemical and FISH testing. *J Clin Pathol* 2004; **57**: 1140–1144.
15. Kononen J, Bubendorf L, Kallioniemi A, *et al*. Tissue microarrays for high-throughput molecular profiling of tumor specimens. *Nat Med* 1998; **4**: 844–847.

16. O'Grady A, Flahavan CM, Kay EW, *et al*. HER-2 analysis in tissue microarrays of archival human breast cancer: comparison of immunohistochemistry and fluorescence in situ hybridization. *Appl Immunohistochem Mol Morphol* 2003; **11**: 177–182.
17. Oladipo O, Conlon S, Grady AO, *et al*. The expression and prognostic impact of CXC-chemokines in stage II and III colorectal cancer epithelial and stromal tissue. *Br J Cancer* 2011; **104**: 480–487.
18. Kay EW, Barry Walsh CJ, *et al*. Inter-observer variation of p53 immunohistochemistry–an assessment of a practical problem and comparison with other studies. *Br J Biomed Sci* 1996; **53**: 101–107.
19. Emmert-Buck MR, Bonner RF, Smith PD, *et al*. Laser capture microdissection. *Science* 1996; **274**: 998–1001.
20. Espina V, Heiby M, Pierobon M, *et al*. Laser capture microdissection technology. *Expert Rev Mol Diagn* 2007; **7**: 647–657.
21. Wulfkuhle JD, Aquino JA, Calvert VS, *et al*. Signal pathway profiling of ovarian cancer from human tissue specimens using reverse-phase protein microarrays. *Proteomics* 2003; **3**: 2085–2090.
22. Sheehan KM, Calvert VS, Kay EW, *et al*. Use of reverse phase protein microarrays and reference standard development for molecular network analysis of metastatic ovarian carcinoma. *Mol Cell Proteomics* 2005; **4**: 346–355.
23. Paweletz CP, Charboneau L, Bichsel VE, *et al*. Reverse phase protein microarrays which capture disease progression show activation of pro-survival pathways at the cancer invasion front. *Oncogene* 2001; **20**: 1981–1989.
24. Liotta LA, Espina V, Mehta AI, *et al*. Protein microarrays: meeting analytical challenges for clinical applications. *Cancer Cell* 2003; **3**: 317–325.
25. Mueller C, Liotta LA, Espina V. Reverse phase protein microarrays advance to use in clinical trials. *Mol Oncol* 2010; **4**: 461–481.
26. Espina V, Wulfkuhle JD, Calvert VS, *et al*. Reverse phase protein microarrays for monitoring biological responses. *Methods Mol Biol* 2007; **383**: 321–336.
27. Gulmann C, Sheehan KM, Kay EW, *et al*. Array-based proteomics: mapping of protein circuitries for diagnostics, prognostics, and therapy guidance in cancer. *J Pathol* 2006; **208**: 595–606.
28. Mueller DC. Reverse Phase Protein Microarray Analysis Suite. Version 1.11 2013. http://capmm.gmu.edu/rpma-analysis-suite.
29. Chiechi A, Mueller C, Boehm KM, *et al*. Improved data normalization methods for reverse phase protein microarray analysis of complex biological samples. *BioTechniques* 2012; **0**: 1–7.
30. Chiechi A, Novello C, Magagnoli G, *et al*. Elevated TNFR1 and serotonin in bone metastasis are correlated with poor survival following bone metastasis diagnosis for both carcinoma and sarcoma primary tumors. *Clin Cancer Res* 2013; **19**: 2473–2485.
31. Taniguchi M, Kitatani K, Kondo T, *et al*. Regulation of Autophagy and Its Associated Cell Death by "Sphingolipid Rheostat": reciprocal role of ceramide and sphingosinnd 1-phosphate in the mammalian target of rapamycin pathway. *J Biol Chem* 2012; **287**: 39898–39910.
32. Fan S, Niu Y, Tan N, *et al*. LASS2 enhances chemosensitivity of breast cancer by counteracting acidic tumor microenvironment through inhibiting activity of V-ATPase proton pump. *Oncogene* 2013; **32**: 1682–1690.
33. Ruckhaberle E, Karn T, Rody A, *et al*. Gene expression of ceramide kinase, galactosyl ceramide synthase and ganglioside GD3 synthase is associated with prognosis in breast cancer. *J Cancer Res Clin Oncol* 2009; **135**: 1005–1013.
34. Maes H, Rubio N, Garg AD, *et al*. Autophagy: shaping the tumor microenvironment and therapeutic response. *Trends Mol Med* 2013; **19**: 428–446.
35. Espina V, Mariani BD, Gallagher RI, *et al*. Malignant precursor cells pre-exist in human breast DCIS and require autophagy for survival. *PLoS One* 2010; **5**: e10240.
36. Yang S, Wang X, Contino G, *et al*. Pancreatic cancers require autophagy for tumor growth. *Genes Dev* 2011; **25**: 717–729.
37. Sentelle RD, Senkal CE, Jiang W, *et al*. Ceramide targets autophagosomes to mitochondria and induces lethal mitophagy. *Nat Chem Biol* 2012; **8**: 831–838.
38. Russo SB, Baicu CF, Van Laer A, *et al*. Ceramide synthase 5 mediates lipid-induced autophagy and hypertrophy in cardiomyocytes. *J Clin Invest* 2012; **122**: 3919–3930.
39. Delgado ME, Dyck L, Laussmann MA, *et al*. Modulation of apoptosis sensitivity through the interplay with autophagic and proteasomal degradation pathways. *Cell Death Dis* 2014; **5**: e1011.
40. Qin Z, Dai L, Trillo-Tinoco J, *et al*. Targeting sphingosine kinase induces apoptosis and tumor regression for KSHV-associated primary effusion lymphoma. *Mol Cancer Ther* 2014; **13**: 154–164.
41. Lavieu G, Scarlatti F, Sala G, *et al*. Regulation of autophagy by sphingosine kinase 1 and its role in cell survival during nutrient starvation. *J Biol Chem* 2006; **281**: 8518–8527.

SUPPLEMENTARY MATERIAL ON THE INTERNET

The following supplementary material may be found in the online version of this article.

Figure S1. Western blot antibody validation for the CerS5 (LS-B3152). Whole-cell lysate was prepared from human colon cancer cell line SW620 and standard western blot analysis with the CerS5 (LS-B3152) antibody was performed.

Figure S2. Box plot diagram showing RPPA expression levels of all 30 endpoints included in the proteomic network analysis. The median (line within the box), mean (centre of the diamond), 25th and 75th percentiles and maximum and minimum values are all displayed on each box-plot.

Table S1. List of primary antibodies used to probe RPPA slides.

Table S2. Relation of CerS5 expression to standard prognostic variables.

Table S3. Normalised relative intensities and total protein for 30 RPPA signalling endpoints.

Table S4. Spearman's Rho correlations for 'IHC CerS5 Low' RPPA measurements.

Table S5. Spearman's Rho correlations for 'IHC CerS5 High' RPPA measurements.